GLARE AT POLITECNICO DI MILANO: EXPERIMENTS AND COMPUTATIONS

Alessandro Airoldi, Paolo Bettini, Luca Lanzi, Giuseppe Sala
Dipartimento di Ingegneria Aerospaziale – Politecnico di Milano
Milan, Italy

Abstract

This work presents the experimental and numerical activities performed at the Dipartimento di Ingegneria Aerospaziale of *Politecnico di Milano with respect to Glare. Glare represents indeed a promising material to manufacture aircraft structural parts when fatigue, damage tolerance and impacts are of primary concern. The paper reports some preliminary results regarding the stiffness, the strength and the impact response of Glare, as well as its peculiar joint technology: the splicing technique. The subsequent activities have been focused on the numerical-experimental investigation of the bucking behaviour of Glare. In this within, a Wagner's web is used. Buckling and post-buckling analyses are performed by using implicit and explicit finite element analyses. An elastic-plastic law was adopted for the aluminium alloy layers of Glare while an elastic model was used for the fibreglass layers. The experiments carried out on the Wagner's web result in good agreement with the numerical computations. Finally, the limits of adopting an elastic model for fibreglass layers are discussed and a constitutive law to model the in-plane inelastic response of Glare is proposed. The theoretical aspects and the calibration of the model are presented and compared with experimental tests. The numerical-experimental correlation proves the reliability of the proposed law, as far as the in-plane inelastic behaviour of Glare is concerned.*

Introduction

Glare (GLAss REinforced aluminium) is a fibre metal laminate (FML) constituted by a cured lay-up of aluminium alloy sheets and glass fiber reinforced layers with epoxy resin systems.
Glare seems a good compromise between pure composite material and pure aluminium alloys and it is now customary accepted as an excellent candidate for the future generation of large aircraft, as it has been already demonstrated by the Airbus' commitment to use Glare for the upper part of the A380 fuselage.
Glare material has a slightly lower specific stiffness than light alloy and is generally lighter than a light alloy sheet of identical stiffness. However its fatigue and damage tolerance properties prove that Glare could be efficiently employed to produce aircraft structures with enhanced impact tolerance performances, high impact strength and energy absorption capabilities [1-6]. Moreover, the so called 'splicing technique' allows to produce very large panels with light alloy sheets of limited size [1-3,7]. The consequent reduction of the economic costs and the good behaviour of the jointed Glare panels [8] represent particularly appealing aspects for the application of Glare in aircraft manufacturing.
On the other hand, aircraft fuselages are customary designed to exploit shear postbuckling capabilities of stiffened panels for weight savings. This design method can be applied only once the initial buckling can be controlled and no plastic deformations or local failures occur. As a matter of fact, this design practice is common and seems to be reliable when metal fuselages are considered.
Accordingly, new accurate design procedures should be developed and validated to use Glare as efficiently as possible. Indeed, when buckling phenomena are considered, more accurate estimations of initial buckling loads, postbuckling stiffness and load levels at which first plastic strains and/or damages occur, will achieve higher structural efficiency and further weight savings. To this regard, design curves have been proposed in [9] as design method for flat stiffened Glare panels by means of detailed finite element analyses accounting for the elastic-plastic behaviour of the aluminium layers.
However, in order to explore the possibilities offered by Glare in the post-buckling field as well as in the developing of impact tolerant structures, numerical models are required to represent the overall behaviour of Glare. The adoption of these models could allow to investigate the response of structural parts beyond the elastic range, to predict the sustainable stress and the risk of localised failures. Consequently, the assessment of a modelling technique and, if needed, of ad hoc constitutive laws to represent the Glare inelastic behaviour are of primary concern.
To investigate the behaviour of Glare laminates a Glare 3-3/2 has been selected as test case for a series of experimental and numerical activities carried out at the *Dipartimento di Ingegneria Aerospaziale* of *Politecnico di Milano*. This type of Glare is constituted by three 0.3 mm thick Al 2024 T3 layers, separated by two fibreglass sublaminates with [0][90] and [90][0] lay-up sequences, respectively.
In the earlier phases of the work, the activities were focused on the technologies required to manufacture Glare laminates and specimens and on the mechanical characterisation of the Glare constitutive materials by static tensile tests.
Accordingly, in the first part of the paper the elastic properties of Glare, its strength and toughness

properties are briefly discussed and illustrated by experimental tests. Aiming to understand its strength properties, some preliminary impact tests are also discussed [6].
Then, the joining technologies developed for Glare material, such as the so called '*splice technology*', are presented [5,7].
Thereafter, the buckling and elastic post-buckling behaviour of Glare laminates is investigated. This preliminary investigation was carried out by using a Wagner's web designed to test couples of Glare flat square panels. Numerical results and experiments are compared and discussed in terms of load-shortening curves, strain levels and post-buckling patterns [10].
Finally the possibility to model the full-range in-plane response of Glare laminates is investigated. The inelastic mechanisms activated in the fiberglass layers are presented analysing the response and the failure modes of different laminates. A constitutive model is developed and implemented for the HKS/Abaqus Explicit code [11]. The numerical-experimental correlation, referred to the full-range response of the $([0][90])_{ns}$ fiberglass specimens and of Glare 3-3/2 is discussed, focusing on the quantitative prediction of the stress vs. strain curves as well as on the qualitative identification of the inelastic mechanisms that influence the behaviour of the laminates.

Assessment of Glare strength, stiffness and toughness properties

The following paragraphs aim at the assessment of the main properties of Glare in terms of its elastic behaviour, strength and toughness properties.

Elastic behaviour

The elastic behaviour of Glare laminates and of its single components are here investigated by means of tensile tests on small specimens. In particular, preliminary tensile tests have been performed on the aluminium alloy sheets and on the fibreglass pre-pregs, separately.
Accordingly, Table 1 summarizes the main elastic properties of the pre-pregs layers of S2 Glass fibers.

Tab. 1: Main properties of the pre-pregs layers of S2 Glass fibers.

E_{11} [GPa]	E_{22} [GPa]	ν_{12}	G_{12} [GPa]	thick. [mm]
45.67	13.6	0.257	5.26	0.23

Since during the Glare manufacturing process, the aluminium alloy sheets are subjected to heat treatment due to the curing process, the characterization tests of the aluminium alloy are performed after an heat treatment at 130° C, corresponding to the curing process. Table 2 reports the main mechanical characteristic of the aluminium sheets, before and after the heat treatment.
The elastic properties of the resulting Glare 3-3/2 panels, as obtained by tensile tests, are reported in Table 3.

Tab. 2: Main properties of the aluminium alloys before and after heat treatment.

	E [GPa]	ν	σ^*_{nl} [MPa]	thick. [mm]
before heat treatment	68.3	0.33	279.1	0.3
after heat treatment	69.8	0.33	304.2	0.3

* stress at 15% deviation from linearity

Tab. 3: Glare 3-3/2 elastic properties.

	E [GPa]	ν	thick. [mm]
Glare 3-3/2	68.3	0.33	1.85

These elastic properties can be compared to those obtained by applying the Classical Lamination theory. If the membrane stiffness matrix of the resulting laminate, with a nominal thickness of 1.82 mm, is divided by the measured thickness of the Glare laminate (1.85 mm), the elastic modulus in the 0° direction turns out to be 49.26 GPa with an error of 4.8% with respect to the experimentally measured value. The expected Poisson Coefficient is 0.270, only 2% higher than the value estimated in the tests.

Strength considerations

Figure 1 presents the full range tensile stress vs. strain curve of a Glare 3-3/2 laminate obtained by means of 5 tests, showing also the standard deviation (STD) of the stress levels at each strain value.
Basing on these experimental data, the specific stiffness and the specific strength of Glare are evaluated together with its own constitutive layers, as reported in Table 3.
Hence, the specific properties of Glare 3-3/2 are intermediate between those of its constitutive layers. In fact, the light alloy has an higher specific stiffness, while the composite cross-ply laminate presents the highest specific strength. However, the curves reported in Fig. 1 exemplify some of the most interesting aspects relevant to the behaviour of Glare in the inelastic range.

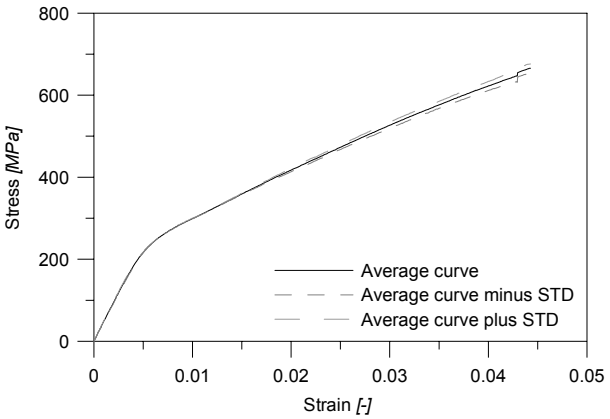

Fig. 1: Glare 3-3/2 tensile stress vs. strain curve.

Tab. 3: Specific stiffness and strength.

	Al 2024 T3	Glare 3-3/2	S2 Glass/Epoxy (cross-ply laminate)
E/ρ [MNm/kg]	24.82	20.59	15.95
σ_R/ρ [MNm/kg]	0.144	0.292	0.432

The deviation from linearity at a strain of about 5% is due the yielding of the light alloy sheets. It can be observed that yielding does not have any apparent influence on the mechanical properties of the composite layers, so that a strain hardening behaviour with a high tangent modulus follows the deviation from linearity. The failure occurs, averagely, at a strain of 4.42%, very close to the strain at failure recorded for S2 Glass/Epoxy laminates. Hence, the strength of the Glass reinforcement is completely exploited in the FML laminate and the ultimate tensile load turns out to be 60% higher than the one that corresponds to a light alloy plate of identical thickness. Moreover, to completely fracture the laminate, the light alloy layers have to be further stretched. On the other hand, the confinement of the composite layers between the metal sheets reduces the effects of brittle failures and progressive damages that can occur in the composite layers. Finally, it is it is worth remarking that no visible delaminations were observed until the final failure of the specimens. Accordingly, the in-plane monotonic tensile response of Glare 3-3/2 until the final failure does not seem significantly influenced by the nucleation or the propagation of interlaminar damages.

Preliminary evaluation of Impact behaviour

The load carrying capability in the inelastic range and the considerable toughness exhibited in the tensile test indicate that one of the most promising characteristic of Glare is its behaviour in impact conditions. Low energy impact tests were performed on Al 2024 T3, cross-ply S2 Glass/Epoxy laminates and Glare 3 3/2 specimens, with a thickness of 1.6 mm, 2.2 mm and 1.8 mm, respectively [6]. An impacting mass of 2.79 kg with a hemispherical impactor having a diameter of 12.5 mm was used. The results are reported in Fig. 2.

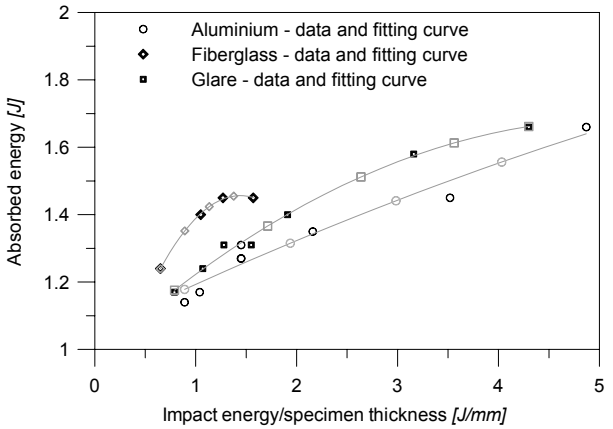

Fig. 2: Absorbed energy levels vs. impact energy in low energy impact tests.

The fiberglass laminates exhibit an high energy absorption efficiency for lower impact energies. Anyhow, the fiberglass laminates are not able to absorb impact energy beyond the 1.5 J/mm level, as they delaminate and undergo brittle fracture processes.
The Glare 3-3/2 curve is always higher than the one of the light alloy at a given impact energy, thus showing its better efficiency.
After the impact, the Glare specimens present an indentation similar to those exhibited by metallic specimens. This aspect represents indeed a fundamental advantage with respect to composite materials, where the damages induced by impacts are very often not visibly detectable. Moreover, the impacted specimens do not show any delaminated area (Fig. 3). Concluding, these impact tests point out the drawbacks derived by the brittleness of the fiberglass composites and confirm the appreciable impact behaviour of Glare, that seems capable to combine the best characteristics of its constitutive layers.

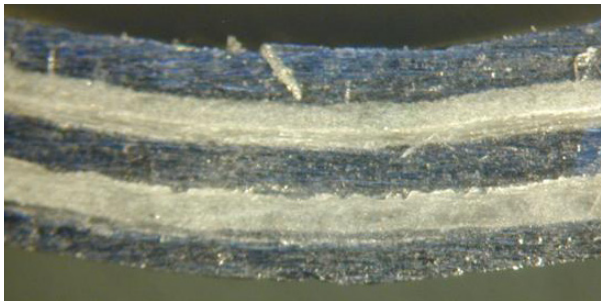

Fig. 3: Section of a Glare 3-3/2 after a low energy impact test

Behaviour of different typologies of joints

The choice of using Glare in aircraft structures can be further evaluated taking into account the behaviour of joined panels.
In fact, Glare characteristics make available peculiar joint technologies, such as the splicing technique [2]. The main advantage of this technique is to obtain very large FML panels, with light alloy sheets of limited size with a single curing process.
Figure 4-A,B and C, show three different possibilities of splice joints, while Fig. 4-D is referred to a typical joints with two doublers.

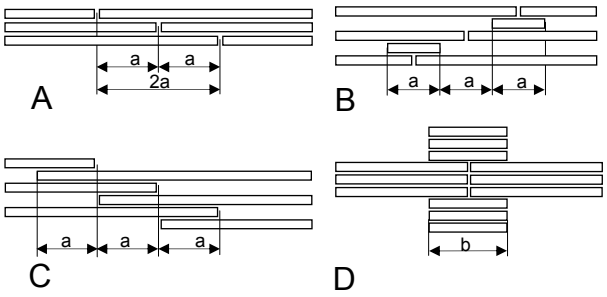

Fig. 4: Different joint configurations tested in the experimental activities.

The four joints presented in Fig. 4 were tested in tension, obtaining the average curves reported in Fig. 5 and compared with the stress vs. strain curve of a reference Glare panel without joints [5,7].
All the splice joints exhibit a tough behaviour, although the simple splice joint indicate a loss of load carrying capability with respect to the reference curve. On the contrary, the doubler joint presents a brittle failure.

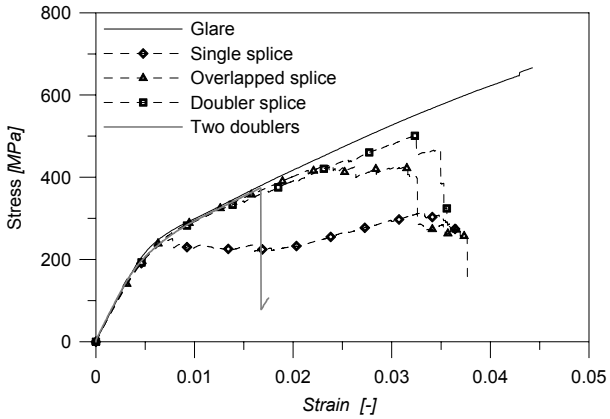

Fig. 5: Tensile response of differently joined Glare panels.

Numerical-experimental behaviour of Glare panels under shear buckling

The previously presented experimental activities point out the good mechanical properties and the enhanced toughness characteristics of Glare panels, also taking into account the behaviour of joints.
Glare seems then a promising material to manufacture aircraft skins with good damage and impact tolerance characteristics. As far as Glare application in aircraft industries is concerned, the buckling strength of Glare panels is of primary concern.
Basing on these considerations, further numerical and experimental activities were performed at *Dipartimento di Ingegneria Aerospaziale* of *Politecnico di Milano*, investigating the buckling behaviour of Glare panels [10].
A Wagner's web was then designed to test couples of Glare flat square panels. Detailed finite element analyses were performed with HKS/Abaqus [12]. Thereafter, preliminary experimental tests have been performed to validate the numerical model.
Numerical results and experiments are finally compared and discussed in terms of load-shortening curves, strain levels and post-buckling patterns.

Considered test case

As sketched in Fig. 6, the Wagner's web consists of two main parts: a couple of external frames and a couple of Glare square panels, inserted between the external frames. The web is loaded in such a way that the panels are subjected to shear load as it happens during a three point bending test.

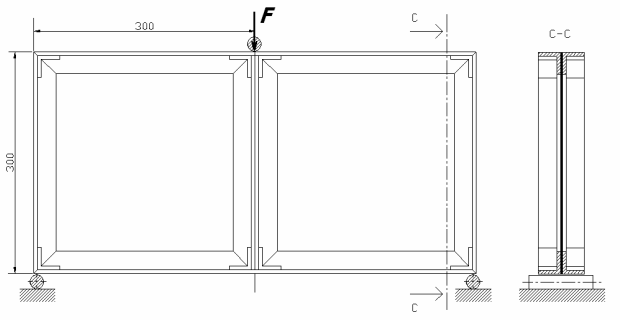

Fig. 6: Wagner's web configuration used for the numerical-experimental correlation.

The external frames of Wager's web are 600 mm wide and 300 mm high. They are made up using L-shaped 6060 aluminium alloy beams with side of 30 mm and thickness of 5 mm. In order to obtain reliable numerical-experimental correlations, a mechanical characterization of the aluminium alloy that constitutes the external frames has been performed.
Glare panels have nominal dimension of 300x300

mm. The free length of the panels is reduced to 240 mm, once they are inserted between the frames.

Numerical computations

Numerical model: The numerical model is made up of disjointed parts: the front and the rear frames and the Glare panels, separately modelled as shown in Fig. 7.

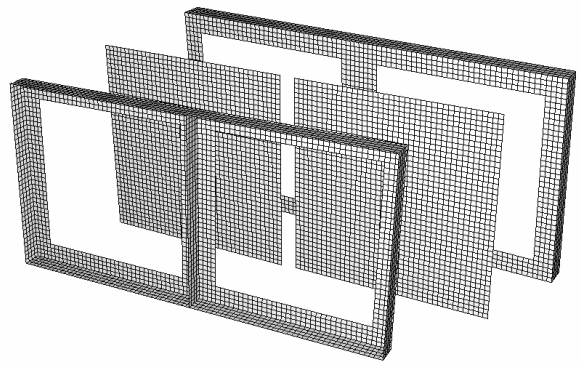

Fig. 7: Finite element model of the Wagner's web: frontal and rear frames, Glare flat panels.

These parts are mutually connected via contact surfaces in order to reproduce the bolted joints between the frame and the inner Glare panels.
The finite element model consists of 8383 nodes and 7747 4-node shell elements with dimension of about 7 mm. The shell elements are of type S4R, with 6 degrees of freedom for each node. Five integration points throughout the shell thickness have been used to model the elements which constitute the front and rear frames, while three integration points in each layer throughout the thickness have been used to model the Glare laminate.
Accordingly to the results and the numerical methods already applied in previous works [13,14], three different kinds of finite element analyses have been carried out. In particular, to investigate the post buckling field, full non-linear finite element analyses have been used, while linearized eigenvalue analyses have been additionally considered to evaluate the first buckling load.
The eigenvalue analysis has been used to evaluate the first buckling load and to return the first eigenmode shape, the static analysis with the modified Riks' method [15,16] has been used to follow the static equilibrium path of a structure in a generalized load-displacement space. Geometrical and material non-linearities are considered using the Newton's method as the basic algorithm. The modified Riks' method has been used to investigate the load-shortening curve and the evolution of buckling phenomena, in terms of deformation, stress and strain, into the post-buckling field. An experienced drawback of the Riks' method is its sensitivity with respect to the choice of the integration step and to the convergence parameters, especially in presence of strong bifurcation points. In fact, a wrong choice of convergence parameters may preclude the ability of the method in following the equilibrium path near the critical load and in the post-buckling field.
A promising way to circumvent such a difficulty and to follow the load vs. shortening curve from the pre-buckling to the post-buckling is the use of dynamic analyses performed with very low displacement velocity so to not be effected by inertial effects [17]. After a preliminary convergence study, the displacement velocity was then fixed at 10 mm/s.
The same boundary conditions, i.e. the same kinematics constraints and loads, were used for all the analyses. In order to prevent lateral displacements of the Wagner's web once that the first buckling load has been reached, later anti-buckling guides have been modelled constraining the lateral translation of the exterior vertical edges of the web.

Numerical results: the results obtained by the three kinds of finite element analyses above described are reported in Table 5.

Tab. 5: Buckling load and required CPU time.

	Buckling load *[kN]*	CPU time *[s]*
Eigenvalue	35.4	116
Riks' method	36.2	1530
Dynamic explicit	34.5	8590

The buckling loads are close together proving the reliability of the obtained results while the comparison between the CPU times shows that the dynamic explicit analysis is the most expensive one.
It is noticed that the static non-linear analysis, with the modified Riks' method, required several tentative runs to tune the convergence parameters so as to properly identify the first buckling load.
The equilibrium path, in terms of the overall load-shortening curve, is drawn in Fig. 8 considering both the dynamic explicit and the Riks' finite element analyses. In this case as well, the obtained results are close enough even if the static analysis, performed with the Riks' method, turns out to have a postbuckling range stiffener than the one predicted by the dynamic explicit analysis.

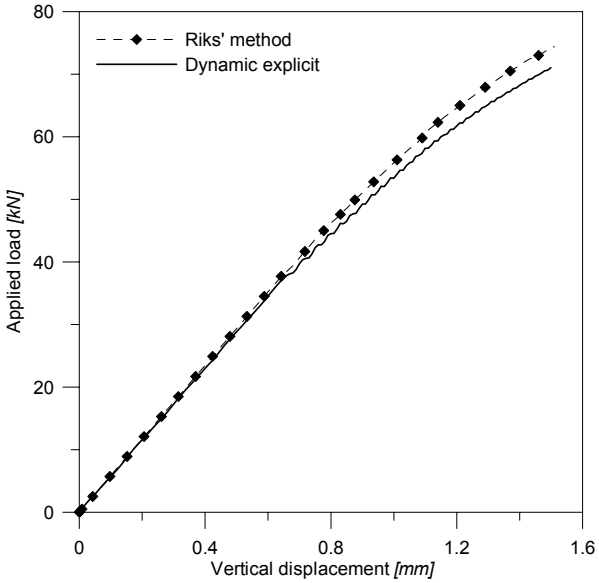

Fig. 8: Load-shortening curves.

As far as the first buckling shape is concerned, all the finite element analyses identified the same buckling pattern. As theoretically expected, the buckling pattern is characterized a single diagonal wave in each bay of the Wagner's web, as shown in Fig. 9.

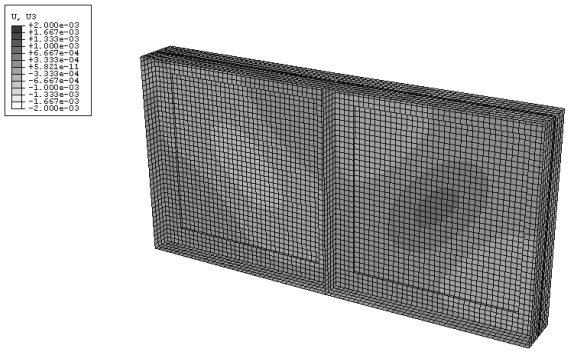

Fig. 9: Out-of-plane deformation at 37 kN.

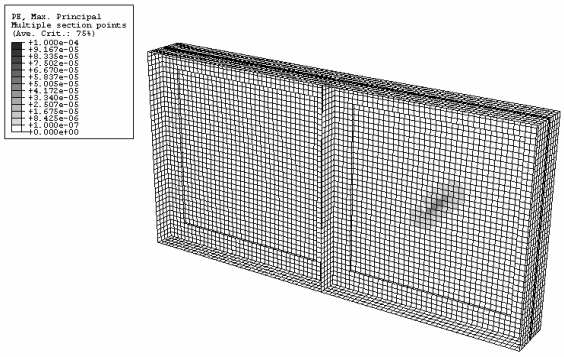

Fig. 10: Plastic strain at 52 kN.

Figure 10 shows the plastic strains distribution in the Wagner's web at 52 kN, proving that no yielding is experienced in the Glare panels up to 52 kN. Accordingly the postbuckling range between 36 and 52 kN exhibits an elastic behaviour.
Even if the analyzed structural typologies is not actually representative of real aircraft stiffened structures, it can be noticed that Glare panels exhibit a wide large postbuckling range before yielding. In fact the ratio between the yielding load and the first buckling load is 1.44 about.

Experimental tests and numerical correlation

Test apparatus: Preliminary experiments were performed in a MTS servo-hydraulic testing system 810 TestStar IIs, provided by an ad hoc clamping frame. Namely, the testing system was provided by a clamping frame designed to constraint the Wagner's web and to apply the bending load by means of three support points. Anti-buckling lateral guides are fixed on the lower beam to prevent lateral displacement of Wagner's web vertical edges. Shear buckling tests were displacement-controlled and performed at a constant vertical displacement velocity of 0.01 mm/s, so as to satisfy as much as possible the ideal static test conditions.
In order to monitor the out-of-plane deformations and to follow the buckling pattern development during the tests, the shadow Moirè [18] optical technique was used. The Moiré shadows were fixed to the clamping frame at a distance of about 2 mm from the panel skin and lighted at 45°.
Since the numerical computations already performed turned out to exhibit buckling waves with small amplitude at the beginning of the postbuckling field, several strain gauges were installed of the Glare panels in order to precisely identify the first buckling load as reported in Fig. 11. During all the experimental tests, the strain values are recorded each 2.5 kN.

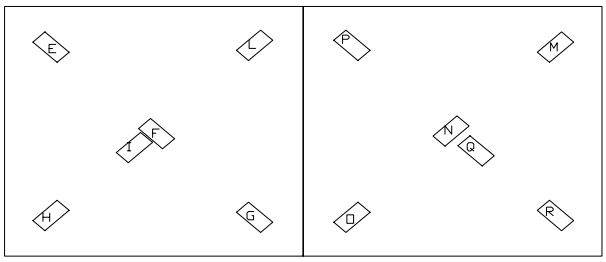

Fig. 11: Locations of the strain gauges on Glare panels.

Test results and numerical correlation: the experimental tests presented in this work were performed up to about 50 kN not to yield the Glare panels. Test results are compared to the values foreside by the previous numerical computations.
The estimation of the first buckling load has made possible by the strain values. Figure 12 reports the

strain values experienced on the compressed diagonal of the panel, namely strain gauges H, I and L in Fig. 11. Similarly, Fig. 13 reports the strain values on the stretched diagonal, namely strain gauges E, F, G on Fig. 11.
It is noticed that in the pre-buckling field the absolute values of the strains along the stretched and compressed diagonals are almost the same, confirming an uniform shear stress distribution in the panels.

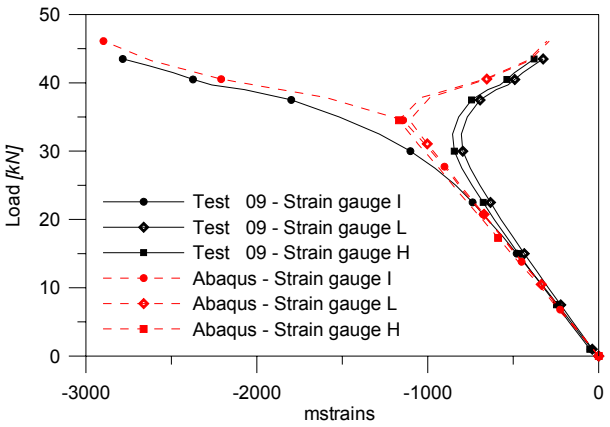

Fig. 12: Strains on the compressed diagonal.

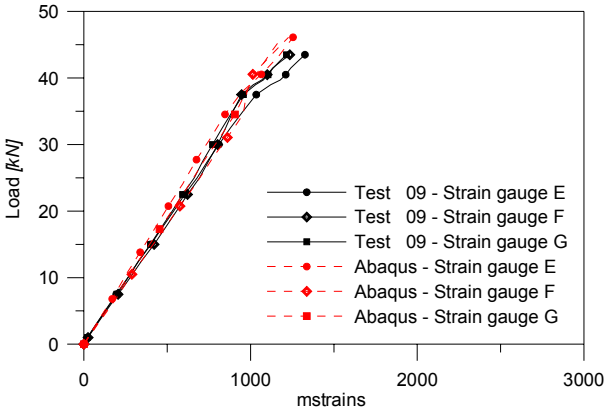

Fig. 13: Strains of the stretched diagonal.

On the contrary, when the first buckling load is reached, the recorded strains tend to separate the ones from the others, as shown in Fig. 12 and 13.
Strain values confirm that, once the first buckling load has been overcome, the Wagner's web begins to operate under diagonal tension. Accordingly, while the strain gauges located on the compressed diagonal drastically separate each other, those located on the stretched diagonal continuously increase with an almost constant slope and remain closer than the compressed ones. The first buckling load is experienced at 32.5 kN, against the 34.5 kN returned by the dynamic explicit analysis, resulting in a percentage error within 6.5%.

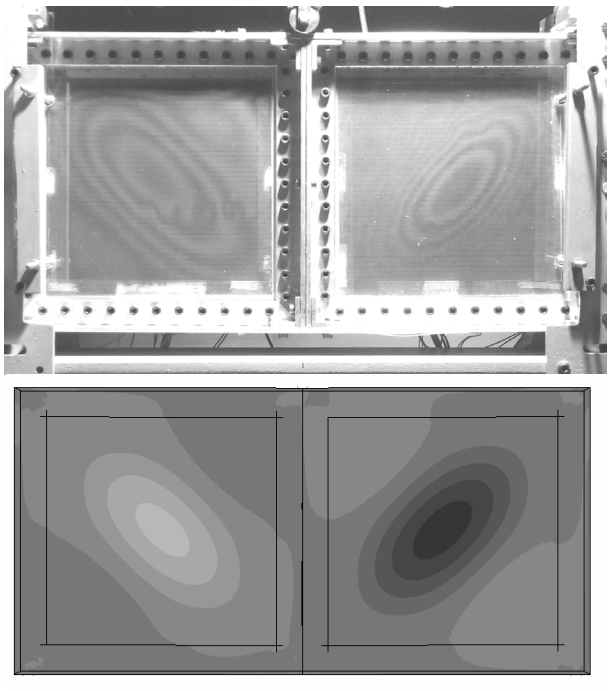

Fig. 14: Out-of-plane deformation at 37.5 kN.

Finally, Fig. 14 compares the out-of-plane deformations obtained by the numerical computation with those visualized by the Moirè fringes during the tests. Also in this case, experiments and computations results close together.

Modelling the in-plane inelastic behaviour of Glare

Limitation of the elastic material model for composite layers

The previously presented analyses were performed using an elastic-plastic law for the metal layers and a orthotropic perfectly elastic material model for the composite plies. Considering the tensile response of a Glare 3-3/2 specimen an experimental numerical correlation was carried out to assess the range of validity of the proposed material characterisation.

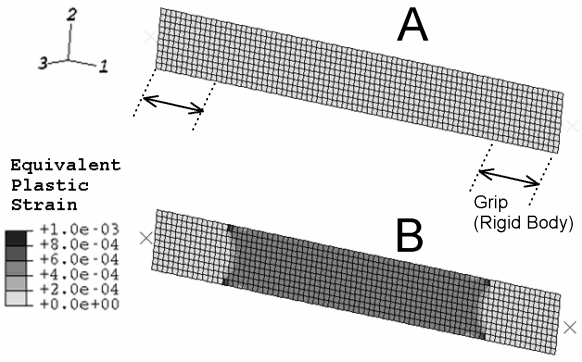

Fig. 15: Model of the Glare 3-3/2 tensile specimen (A) and analysis (B).

The results shown in Fig. 16-A indicate that the model overestimates the load carrying capability in the non-linear range. Moreover, in the initial part of the response, the deviation from the linearity shown by the experimental curve is more progressive than the numerical one. These aspects could be neglected in the evaluation of the first buckling loads, although the identification of the margins of safety with respect to the onset of plastic deformation or to the final panel collapse could be only roughly estimated without properly modelling the full-range response of the laminate.

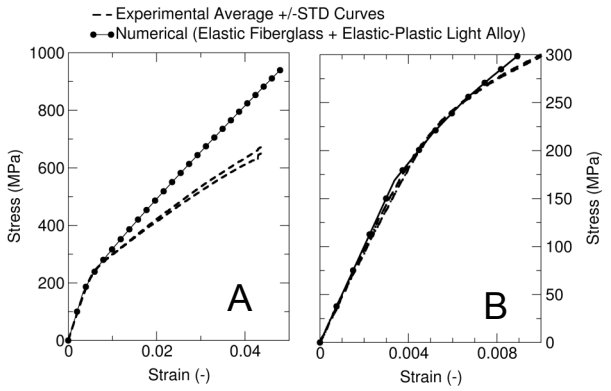

Fig. 16: Numerical-experimental correlation of the Glare 3 3/2 tensile behaviour using an elastic fiberglass model.

On the other hand, the overestimation of Glare inelastic response in Fig. 16 is certainly not acceptable as far as the impact behaviour of Glare panel is concerned.
The development of a constitutive law suitable to represent the inelastic mechanisms activated in the fiberglass layers was then carried out, starting with the experimental investigation of the fiberglass full-range response [11].

Inelastic mechanisms in fiberglass behaviour

The inelastic behaviour and the failure mechanisms of the composite layers were evaluated by means of quasi-static tensile tests performed on $[0]_n$, $[90]_n$, $([+45][-45])_{ns}$ laminates. Tests on cross-ply laminates were also performed, using a $([0][90])_{ns}$ lay-up. The tests were carried out according the ASTM standards [19,20].
The experimental results show the different failure modes, reported in Fig. 17, and the multiple inelastic mechanisms that characterise the response of fiberglass laminates. The full-range responses of the laminates are presented in Fig. 18, considering the standard deviation of the stress vs. strain curves recorded in the different tests.
The matrix-dominated behaviour of $[90]_n$ laminates is linear and the average strain at failure is very low, compared to the results of the other tests (0.25%). The failure is characterised by a neat intralaminar fracture, parallel to the fibre direction, as shown in Fig. 17-A. The response of the angle–ply laminates, with a $([+45][-45])_{ns}$ lay-up, is as well matrix dominated, but in this case the response is highly non-linear. The failure occurs at very high value of strain (about 8%) and it is characterised by the development of a 45° inclined fracture bands, shown in Fig. 17-B.

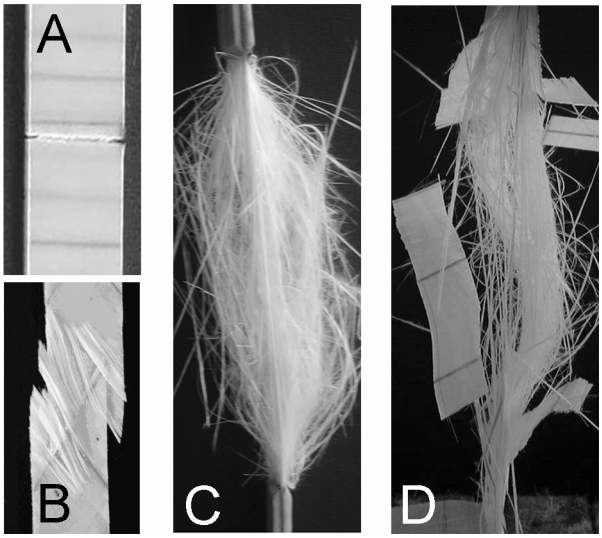

Fig. 17: Failure modes of different fiberglass laminates.

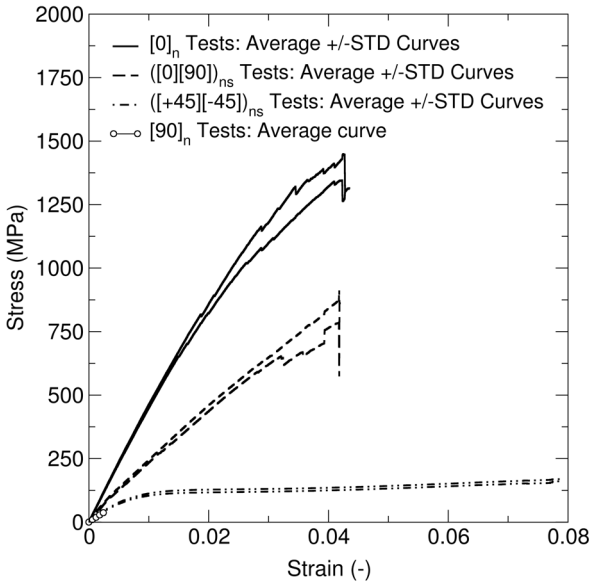

Fig. 18: Stress-strain curves of different fiberglass laminates.

Considering the fibre-dominated responses, the curves reported in Fig. 18 indicate that the response of $[0]_n$ laminates is not completely linear. Beyond the 2% the tangent modulus is progressively reduced. This behaviour is partially

determined by the subsequent failures of groups of fibres, as it is also evidenced by the discontinuities in the average curves. The final failure occur above a strain of 4% when most of the fibres snaps and forms a twisted and tangled mass that does not allow to identify any clear fracture line across the specimen width, as shown in Fig. 17-C. Due to the occurrence of subsequent brittle breakages beyond the 2% strain, the scattering of the stress vs. strain curves is not negligible. On the other hand, the scattering referred to the strain at the final failure is limited, as an average value of 4.34% has been obtained with a standard deviation of 0.30%. In the $([0][90])_{ns}$ specimens, the failure can be as well attributed to the breakage of the 0° fibres, as in the $[0]_n$ laminates. The strain at failure is similar, as an average value of 4.18% has been recorded, with a standard deviation of 0.25%. In the failed specimens, the 90° oriented plies appear apparently undamaged, as shown in Fig. 17-D, although the development of a pattern of transverse matrix cracks can be clearly revealed by a closer inspection. Actually, the cracking of these plies also influences the overall response of the laminate.

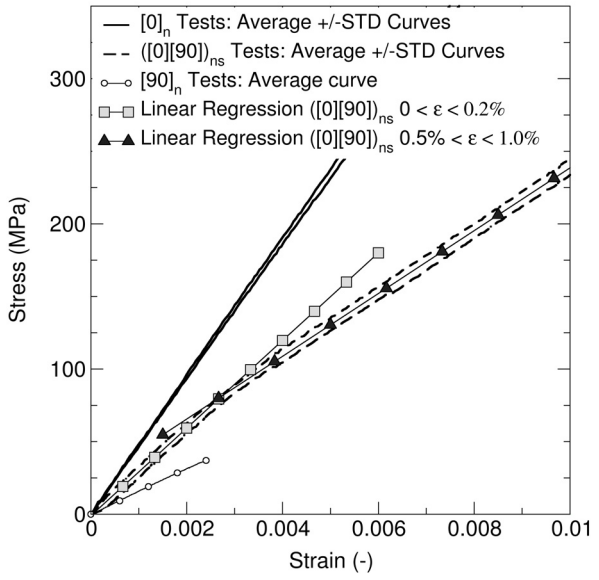

Fig. 19: Bi-linear response of $([0][90])_{ns}$ fiberglass laminates.

Fig. 19 shows the initial part of the responses for the $[0]_n$, $([0][90])_{ns}$ and $[90]_n$ laminates until a strain of 1%. The curves referred to the $([0][90])_{ns}$ laminates present an evident bi-linear behaviour. The strain at the intersection between the two linear regressions indicated in Fig. 19 is 0.27%, that is only slightly higher than the average ultimate strain of the $[90]_n$ specimens (0.25%). According to these observations, it can be concluded that the 90 deg oriented plies in the ([0][90])ns lay-ups are progressively damaged by the development of transverse matrix cracks that occurs at a strain ε_{22} comparable to the strain at failure of [90]n laminates. As the 0 deg plies can easily supply to the damage of the 90 deg plies, matrix cracking do not imply the failure of the specimen but progressively diffuses along the 90 deg plies, until a typical damage state is reached [21].

Development of a constitutive law to model the fiberglass layers

The experimental results point out the multiple inelastic mechanisms that can be activated in the fiberglass layers subjected to tensile loads. Particularly, the analysis of the experimental data allows to introduce a distinction between inelastic processes that depend on the behaviour of to the reinforcement fibres and the ones that are mainly influenced by the response of the resin and of the resin/fibre interface.

These observations indicate that a biphasic material model could be able to adequately represent, in finite element analyses, the non-linearities and the failure modes of the composite layers that constitutes a Glare laminate. A model of this type has been developed and interfaced with the HKS/Abaqus Explicit code at *Dipartimento di Ingegneria Aerospaziale* of *Politecnico di Milano*, to model the progressive damage in composite material basing on a biphasic approach [22]. The material model will be hereby reviewed and applied to the fiberglass layers considered in this work.

A biphasic orthotropic material model allows to express the average stress on a representative volume element of composite material as the sum of two separate contributions. The first contribution represents the average axial stress sustained by the fibres bundles, the fibre phase, while the second accounts for the average stress in the surrounding matrix phase.

The non-linear matrix dominated material responses, as well as the brittle reinforcement failure processes, can be modelled in the constitutive law by degrading the elastic properties of the idealised phases with damage state variables. The introduction of a continuum damage mechanics formulation for both fibre and matrix idealised phases is hereby carried out for a composite with two mutually orthogonal fibre reinforcement directions, in plane stress states. By introducing the damage variables referred to the fibre phases, d_{if} ,and to the matrix phase, d_m, the constitutive relationships can be conveniently expressed in matrix notation, as reported in Eq. 1.

$$\begin{Bmatrix}\sigma_{11}\\ \sigma_{22}\\ \sigma_{12}\end{Bmatrix} = \left(\begin{bmatrix} E_1^f v_1^f (1-d_1^f) & 0 & 0 \\ 0 & E_2^f v_2^f (1-d_2^f) & 0 \\ 0 & 0 & 0 \end{bmatrix} + \right.$$
$$\left. + \begin{bmatrix} C^m_{1111} & C^m_{1122} & 0 \\ C^m_{2211} & C^m_{2222} & 0 \\ 0 & 0 & C^m_{1212} \end{bmatrix} (1-d^m) \right) \begin{Bmatrix}\varepsilon_{11}\\ \varepsilon_{22}\\ \gamma_{12}\end{Bmatrix}$$

Eq. 1

where E_{if} are the effective elastic moduli of the fibres, v_{if} the corresponding fibre volumetric fractions, and C^m_{ijhk} represent the components of the stiffness tensor of the matrix phase.

The evolution of the single scalar damage parameter d_m is introduced to model the matrix-dominated non-linear responses, taking into account the toughness properties related to the resin and resin/fibre interface behaviour. The capability of this single parameter to model the non-linearity of an anisotropic material is enhanced by the introduction of an anisotropic initial damage criterion. The adopted initial damage threshold function, presented in Eq. 2, is then formulated in analogy with the Tsai-Hill anisotropic strength criterion for plane stress states.

$$f^{md}(\bar{\varepsilon}) = \left[\left(\frac{\bar{\varepsilon}_{11}^2}{e_1^2} - \frac{\bar{\varepsilon}_{11}\bar{\varepsilon}_{22}}{e_1^2} + \frac{\bar{\varepsilon}_{22}^2}{e_2^2} + \frac{\bar{\varepsilon}_{12}^2}{e_{12}^2} \right) - 1 \right] = \left[\tilde{\varepsilon} - 1 \right] = 0$$

Eq. 2

The three material parameters e_1, e_2, and e_3 in Eq. 2 identify the limit of elastic behaviour of the idealised matrix phase and the equivalent strain $\tilde{\varepsilon}$ represent a scalar equivalent strain variable.

The evolution law of the matrix phase damage is as well expressed as a function of the equivalent strain previously defined. A suitable form of the matrix damage law was found by using a non-linear piecewise approximation.

Analogously to the matrix phase, a damage increment threshold function was introduced for the fibres in different directions. In this case, the damage was considered simply dependent on the strain component in material axes corresponding to the reinforcement direction, ε_{fi}. A simple linear piecewise damage evolution law has been chosen to model the brittle failure processes that characterise the reinforcement. Damage onset is set at a strain of e_{i0f}. Damage values of d_{i1f} and d_{i2f} are obtained at $\varepsilon_{fi} = e_{i1f}$ and $\varepsilon_{fi} = e_{i2f}$.

Calibration of the constitutive law

The data derived from the tests preformed on fiberglass laminates with $[0]_n$, $[90]_n$, $([+45][-45])_{ns}$ lay-ups were used to calibrate the developed material model.

The first step in the calibration process is the decomposition of the elastic properties into the two idealised material phases. The biphasic model tries to describe the material behaviour as closely as possible from the physical point of view, with the minimum number of internal state variables. Following this consideration, the decomposition of the material properties has to represent an acceptable approximation of the true reinforcement modulus, while the idealised matrix phase is required to model the matrix dominated properties of the composite. It has been found that a decomposition scheme introduced in based on the knowledge of the effective reinforcement modulus can lead to a poor and unrealistic characterisation of the idealised matrix phase properties, if the effective reinforcement moduli E_{if} are not known with great accuracy. A different decomposition strategy has been developed in [22], basing on the control of the matrix phase properties. The decomposition procedure gives as a result a value of the effective reinforcement moduli that can be compared to the bare fibre modulus. It is worth noting that, on the basis of theoretical considerations [23], the effective reinforcement moduli should not be higher than the bare fibre modulus.

The decomposition algorithm described in [22] was applied to the fiberglass stiffness tensor derived by the experimental data considering a fibre volumetric fraction of 0.5, with the results reported in Eq. 3, where the stiffness components are given in GPa.

$$C = \begin{bmatrix} 46.59 & 3.565 & 0 \\ 3.565 & 13.87 & 0 \\ 0 & 0 & 5.126 \end{bmatrix}$$

$$C^f = \begin{bmatrix} 37.67 & 0 & 0 \\ 0 & 0 & 0 \\ 0 & 0 & 0 \end{bmatrix}; \; C^m = \begin{bmatrix} 8.91 & 3.56 & 0 \\ 3.56 & 13.87 & 0 \\ 0 & 0 & 5.126 \end{bmatrix}$$

Eq. 3

The effective elastic moduli of the reinforcement turns out to be 75.34 MPa, 11% lower than the bare fibre modulus declared for the S2 glass fibres.

To calibrate the damage laws, the limits of the elastic behaviour of the matrix phase were chosen analysing the full-range response of the composite. The values adopted are reported in Fig. 20. Then, the evolution damage law of the matrix was tuned to match the highly non-linear response of the $([+45][-45])_{ns}$ laminates. The calibration was verified with the HKS/Abaqus Explicit code using a model constituted of a single layered shell in pure monoaxial tension. Figure 21 shows the numerical-experimental correlation of the stress vs. strain curves for the $([+45][-45])_{ns}$ laminates and the evolution of the numerical matrix damage in a ply.

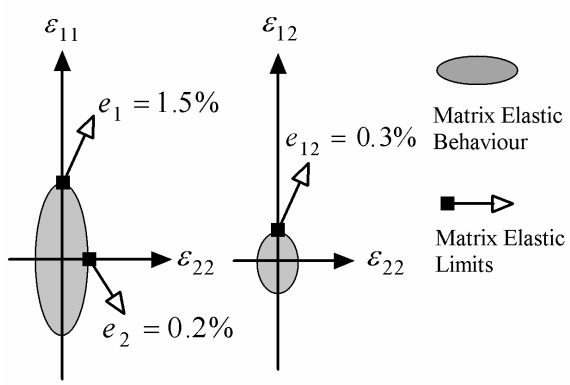

Fig. 20: Calibration of the limits of the elastic behaviour for the matrix phase.

The damage of the fibre phase was calibrated to take into account the final failure beyond the 4.0% strain level as well as the progressive failures of groups of fibres that had been observed in the [0]n tests. The onset of damage was set at ε_{11} = 2.5% and a progressive increment until d_f = 0.15 was introduced until ε_{11} = 4.1%. At ε_{11} = 4.2% the damage is increased up to 0.99, to represent the final failure process.

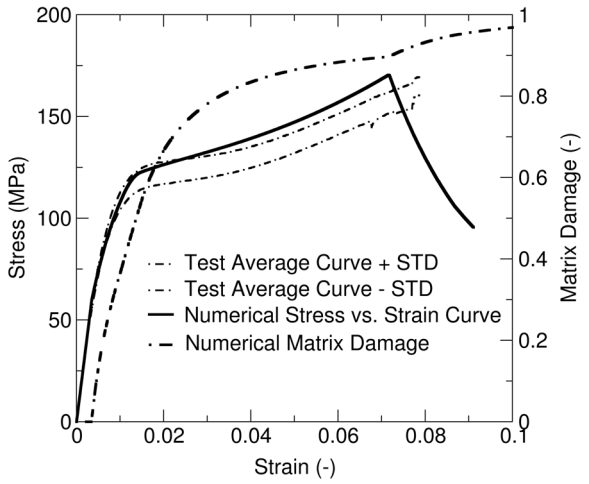

Fig. 21: Numerical-experimental correlation and numerical damage of the ([+45][-45])ns lay-up response.

Fig. 22 reports the verification of the calibrated constitutive law obtained using the single shell model with the $[0]_n$, $[90]_n$, $([+45][-45])_{ns}$ lay-up and comparing the results with the corresponding experimental responses.

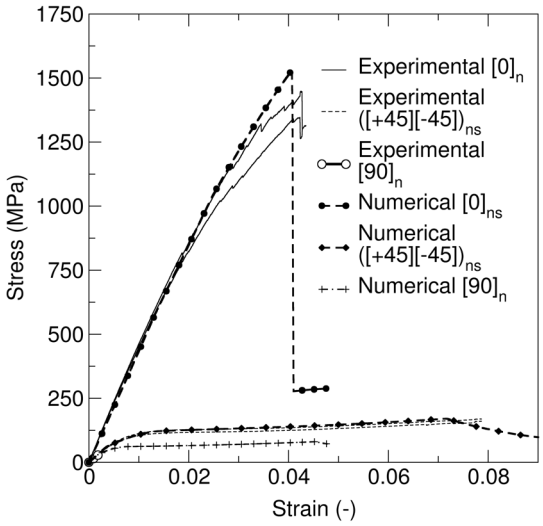

Fig. 22: Verification of the calibrated material model with the numerical-experimental correlation for the $[0]_n$, $[90]_n$, $([+45][-45])_{ns}$ tests.

Although the adoption of a single damage variable for the matrix phase does not allow to model the brittle failure of the $[90]_n$ laminates, the calibrate material model appears capable to represent with acceptable accuracy the different inelastic mechanism that characterise the fiberglass response.

The constitutive law was then applied to correlate the numerical tensile response of a $([0][90])_{ns}$ lay-up with the experimental data. The results, reported in Fig. 23-A, indicate that the initial part of the curve is accurately reproduced, confirming the consistency of the characterisation in the elastic range. As shown in Fig. 23-B, a numerical matrix damage starts developing at a strain level of 0.2% in the 90° oriented plies, inducing a reduction of the curve slope. Fig. 23 also shows that, at strain levels beyond 1.5%, the slope of the numerical curve is reduced by the matrix damage in the 0° oriented plies, and then by the progressive damage introduced in the response of the fibre phase of these plies. At a strain of about 4% the fibre phase of the 0° oriented plies completely fails in the model and the matrix in the 90° oriented plies is strongly degraded, while the reinforcement fibres in these plies are not yet damaged, in accordance with the experimental evidence.

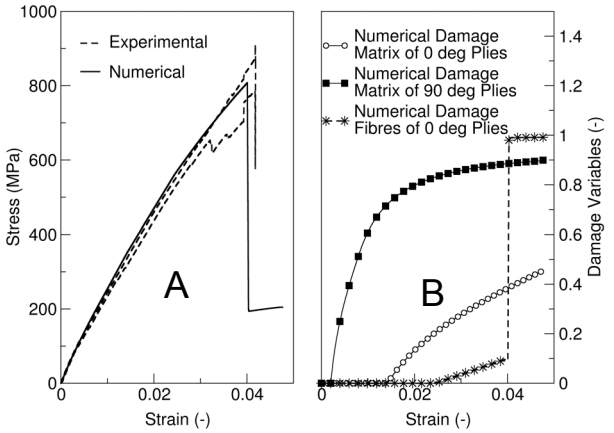

Fig. 23: Numerical-Experimental correlation of the tensile response for ([0][90])ns lay-up (A) and numerical damage variables in the different plies (B).

Numerical-experimental correlation of Glare 3-3/2 inelastic response

Figure 24 reports the numerical-experimental correlation obtained introducing the developed and calibrated constitutive law in the model of the Glare 3-3/2 tensile specimen. Initially, the material model of light alloy plies has been calibrated according to the response of Al 2024 T3 sheet before the heat treatment corresponding to the curing process. The stress levels carried by the modelled laminate beyond the yielding of the light alloy sheet are significantly decreased with respect to the adoption of a purely elastic material for the fiberglass layers. After the yielding of the metal sheets, the numerical stress level turns out to be underestimated with respect to the experiments, with a discrepancy that increases with the strain and that varies between 8% and 12%. Thereafter, two further modifications were introduced in the calibrated material models assigned to the plies. The response of the Al2024-T3 sheets after the heat treatment equivalent to the curing process was considered for the metal plies. Moreover, the reduced scattering and the absence of progressive brittle failures in the experimental response of Glare specimens were taken into account. These observation were interpreted as an indication that the confinement of the composite layers between the metal sheets reduces the occurrence of scattered failures in the reinforcement phase. For this reason the progressive damage of the fibre, originally set at a 2.5% longitudinal strain level, was eliminated and only the final brittle failure was modelled for the fibre phase in the calibrated constitutive law. The numerical results obtained with these two modifications present an appreciable correlation with the experimental ones, as shown in Fig. 24.

As far as the initial part of the response is concerned, the numerical stress-strain curve is very close to the experimental response until the yielding of the metal layers. The shape of the curve in the non-linear range is correctly represented until the failure, although the stress level in the fully developed non-linear range is generally underestimated of about 5%.

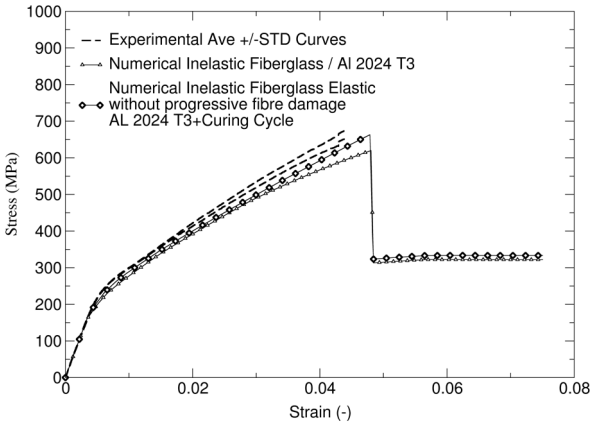

Fig. 24: Numerical-Experimental correlation of the full-range (A) response of Glare 3-3/2 obtained with inelastic composite layers.

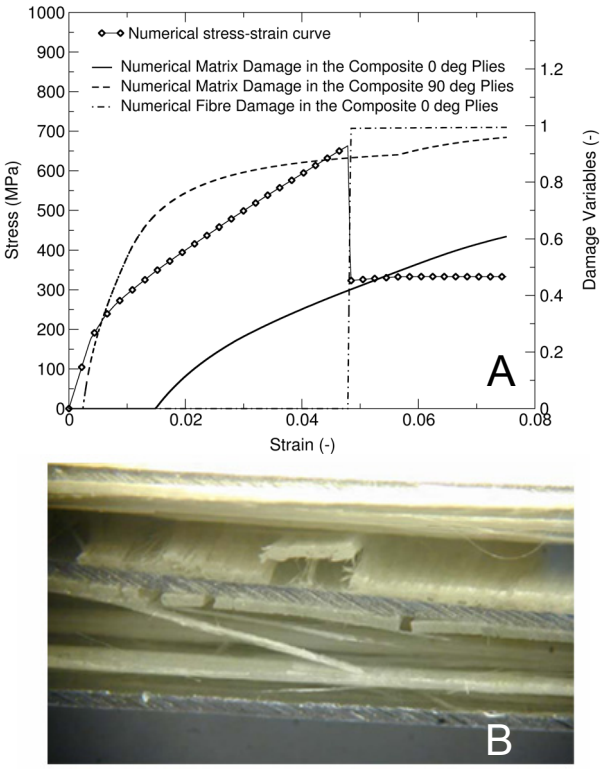

Fig. 25: Evolution of the damage variables obtained with the material model developed for the composite plies (A) and experimental damage observed in a failed Glare specimen (B).

Fig. 25 reports the numerical stress-strain curve referred to this analysis and the evolution of the damage variables that can be compared with the damage modes observed in a failed specimen of Glare 3-3/2.
The numerical analysis models the development of transverse matrix cracking in the 90° oriented plies at a strain level of 0.25%. Thereafter, the light alloy sheets yield at a strain of about 0.5%. At higher strain levels, the response is influenced by the strain hardening of the metal layers and by the inelastic mechanisms activated in the 0° oriented plies. Considering the appreciable numerical-experimental correlation of the full-range stress-strain response, the developed model appears a promising numerical tool to predict the onset and the development of the most relevant inelastic mechanism that can influence the overall in-plane response of Glare laminates.

Conclusions

The experimental activities presented in the first part of the paper confirmed the high fracture energy that characterises the Glare panels, as well as the peculiar toughness properties of Glare structures when joined by means of splice junctions.
The numerical and experimental studies carried out regarding the post buckling behaviour of Glare panels clearly indicate that the undamaged Glare panel have a wide post-buckling elastic range. Considering the significant strain hardening exhibited by Glare in-plane behaviour, it can be affirmed that Glare panels could be capable to withstand buckling load even when damaged by local impacts.
Hence, Glare seems a promising material to manufacture aircraft structures with enhanced damage and impact tolerance properties.
In particular, the appreciable impact behaviour of Glare could be properly exploited in those parts of the rotorcraft structures which are the most exposed to the risk of different types of impacts. Possible applications include the cockpit frames, which have to be designed to withstand to severe bird impact conditions according to the current regulations. The application of Glare to the lower skin of the helicopter hull deserves as well to be investigated. As a matter of fact, ditching loads, characterised by high pressures applied to the skin panels, could be properly transmitted by Glare panels to the internal subfloor frame with a limited risk of perforations.
As far as the preliminary assessment of these and of others possible applications is concerned, the numerical approaches developed up to now at the *Dipartimento di Ingegneria Aerospaziale* of *Politecnico di Milano* could represent an alternative to extensive experimental tests.
Basing on these considerations, future numerical activities will be focused to better predict and investigate the inelastic behaviour and the failure modes experienced by Glare structures undergoing severe load conditions, such as post-buckling and impacts.
To accomplish such objective, numerical and experimental activities are currently being performed to model delamination onset and propagation within explicit finite element analyses.

Acknowledgements

This work was partly supported by MIUR (Italian Ministry for University and Research). The information in this paper is provided as is and no guarantee or warranty is given. The user thereof uses the information at his sole risk and liability.

References

1. Vlot, A., Gunnink, J. W., Fibre Metal Laminates an introduction, 1st ed, Vol 2, Kluwer Academic Publishers, 2001.
2. Gunnink, J. W., Vlot, A., De Vries, T. J., Van Der Hoeven, W., “GLARE technology development 1997-2000”, Applied Composite Materials, 2002, pp. 201-219.
3. Sinke, J., “Manufacturing of GLARE parts and structures”, Applied Composite Materials, 1963, pp. 293-305.
4. Borgonje, B., Ypma, M. S., “Long term behavior of GLARE”, Applied Composite Materials, 2003, pp. 243-255.
5. Sala, G., Bettini, P., “Problematiche di Fatica del Glare e delle sue Giunzioni Studiate presso il Dipartimento di Ingegneria Aerospaziale nel Biennio 2003-04”, Proceedings of the XII Convegno AIFA, Milan, Italy, March 2005.
6. Bettini, P, Sala, G., “Resistenza Ambientale ed all’Impatto di Componenti Aeronautici in Glare”, Proceeding of the XVIII Congresso Nazionale AIDAA, Volterra, Italy, 19-22 September 2005.
7. Bettini, P, Sala, G., “Tecniche di Giunzione e Riparazione di Laminati in Glare”, Proceeding of the XVIII Congresso Nazionale AIDAA, Volterra (Pisa), 19-22 September 2005.
8. De Vries, T. J., Vlot, A., Hashagen, F., “Delamination behavior of spliced Fiber Metal Laminates. Experimental result”, Composite Structures, No. 46, 1999, pp. 131-145.
9. Wittemberg, T.C., van Baten, T.J., “Parametric Design Curves for Shear Buckling of Flat Orthotropic Stiffened Panels with Application to Glare Material”, Proceedings of the 45th AIAA/ASME/ASCE/AHS Structure, Structural Dynamics and Materials Conference, Palm Springs, California, 2004, AIAA 2004-2054.
10. Lanzi, L., Sala, G., Vanzulli, C., “Postbuckling Behaviour of Glare under Shear: Computations and Experiments”, Proceedings

of the 46th AIAA/ASME/ASCE/AHS Structure, Structural Dynamics and Materials Conference, Austin, Texas, 2005, AIAA 2005-2109.
11. Airoldi, A, Sala, G., "Experimental Investigation and Numerical Modelling of Glare Inelastic behaviour", Proceeding of the XVIII Congresso Nazionale AIDAA, Volterra, Italy, 19-22 September 2005.
12. ABAQUS® Theory and Users' manuals. Hibbitt, Karlsson & Sorensen. Pawtucket U.S.A. 1998.
13. Lanzi, L., "A numerical and experimental investigation on composite stiffened panels into postbuckling," *Journal of Thin-Walled Structures*, Vol. 42, 2004, 1645-1664.
14. Lanzi, L., Bisagni, C., Cordisco, P., "Post-buckling design and testing of stiffened composite cylinders under torsion," *29th European Rotorcraft Forum,* Friedrichshafen, Germany, 2003.
15. Riks, E., "An incremental approach to the solution of snapping and buckling problem," *Int. J. of Solids and Structures*, Vol. 15, 1979, pp. 529-552.
16. Cerini, M., Falzon, B.G., "The Reliability of the Arc-Length Method in the Analysis of Mode-Jumping Problems," *44th AIAA/ASME/ASCE/ AHS Structure, Structural Dynamics and Materials*, Norfolk, Virginia, 2003, AIAA 2003-1621.
17 Lanzi, L., "Composite stiffened panels in postbuckling: experiments and dynamic explicit analyses with LS-DYNA," *30th European Rotorcraft Forum,* Marseille, France, 2004.
18. Theocaris P.S., Moirè fringes in strain analysis. Oxford: Pergamon Press, 1969.
19. ASTM D 3518/D 3518M, Standard Test for In-Plane Shear Response of Polymer Matrix Composite Materials by Tensile Test of a +/-45° Laminate, ASTM International, West Conshohocken, U.S.A., 2001.
20. ASTM D3039/D 3039M, Standard Test Method for Tensile Properties of Polymer Matrix Composite Materials, ASTM International, West Conshohocken, U.S.A., 2000.
21. Reifsnider, K.L., Henneke, E.G., Stinchcomb, W.W., Defect propery relationship in composite materials, AFML TR 76-31. part IV, 1979.
22. Airoldi, A., "A constitutive law for progressive damage in composite materials", PhD thesis, Dipartimento di Ingegneria Aerospaziale, Politecnico di Milano, 2002.
23. Jones, R., Mechanics of Composite Materials, Hemisphere Publishing Corp., New York, U.S.A., 1975.